7. Y. Gaoni and R. Mechoulam, *J. Am. Chem. Soc.*, **93**, 217 (1972).
8. B. Cardillo, L. Merlini, and S. Servi, *Tetrahedron Lett.*, 945 (1972).
9. (a) R. K. Razdan, H. C. Dalzell, nd G. R. Handrick, *J. Am. Chem. Soc.*, **96**, 5860 (1974); (b) S. J. Dominiani, C. W. Ryan, and C. N. Dearmitt, *J. Org. Chem.*, **42**, 344 (1977).

The Electronic Structure of Methanethiol Adsorbed on Silver Surface: An Extended Hückel Study

Sungu Hwang, Yun Hee Jang, and Hojing Kim*

Department of Chemistry, Seoul National University, Seoul 151-742. *Received May 20, 1991*

The adsorption of methanethiol on a Ag(100) surface has been studied with Extended Hückel calculation in the cluster approximation of the substrate. Since it has been known that methanethiol is chemisorbed dissociatively on silver surface by rupture of S-H bond, the methanethiolate radical is taken as adsorbate. Of the various adsorption sites, the 4-fold hollow site is preferred. The methanethiolate radical is mainly adsorbed *via* its 2*e* orbital. The charge transfer from metal to this level leads to the C-S bond weakening, which is consistent with the red shift of C-S stretching mode in surface enhanced Raman (SER) spectrum.

Introduction

Understanding the interactions between thiols and various metals has been of a great concern in catalytic chemistry.[1-15] The thiol adsorption on noble metals has been a subject of much investigation since thiols show the surface-enhanced Raman scattering (SERS) phenomena. Among the various noble metals, silver is extensively studied.[1-8]

We carried out Extended Hückel (EH) calculation on some aliphatic thiols-methanethiol, ethanethiol, 1-propanethiol, and 1-buthanethiol- and found that they have similar energy and nature of HOMO, which is considered to play a central role in bonding to metal surfaces. Details are given in the Appendix. Thus the survey of the adsorption of methanethiol, which is the simplest thiol, on silver surface is motivated to understand the nature of the adsorption of thiol compounds on silver surface.

The adsorption of methanethiol on the transition metal surfaces has been a subject for numerous experimental investigations. The SERS experiment of methanethiol (CH_3SH) adsorbed on silver showed that the adsorbate is chemisorbed dissociatively on metal surface by rupture of its S-H bond.[1-7] From the high-resolution electron energy loss (HREELS) and near-edge X-ray fine structure (NEXAFS) spectrum, Koestner found that the dehydrogenation of the adsorbate on a Pt(111) surface results in formation (CH_3S) and that the thiomethoxy is adsorbed with a highly tilted S-C bond ($45\pm 10°$).[9] The dissociative adsorption mechanism was confirmed from the EELS and thermal desorption (TDS) experiments on a Cu(100) surface.[10] Angle resolved ultraviolet photoelectron spectroscopy (ARUPS) and NEXAFS revealed that the C-S bond of CH_3S is tilted about 30° from the surface normal on a Cu(111) surface.[11]

In present EH calculation for the methanethiol on silver surface, the experimental results described above are used in fixing the adsorption geometry.

We use a cluster model to represent metal surface. Since the chemisorption is regarded as a local phnomenon, *i.e.*, an adsorbate is essentially coupled to only a small number of neighbouring metal atoms, our cluster approach is logically reasonable.[15,16] Moreover, since the SERS phenomena has been known to occur on the rough suface[17-19] or the colloid of a finite dimension,[1-8] the cluster model calculation is adequate to describe the chemistry of the SERS properties than the band calculation. But the results using the cluster model do not seem to converge rapidly with its size increasing and we take as large silver clusters as possible.[15,16]

In the present work, we concentrate on a Ag(100) plane. However, some results on the (110) and (111) planes are presented. Since the higher Miller planes can be described by the combination of the simple Miller planes, this work can be generalized, with some modification, to the higher Miller indices. Although the EH formalism is not very quantitative in nature, it still retains its computational simplicity, ease of interpretation of result, and reasonable computationl time for the calculations on large molecules.

We carry out the fragment orbital (FMO) analysis to see the change of MO of adsorbate due to adsorption. In the FMO analysis, as the basis of the composite system (adsorbate-substrate), AO of each atom is transformed into MO of each fragment (adsorbate and substrate before adsorption). The fragment orbitals serve as the basis of the adsorbate-substrate system.

We also apply consistently the language and formalism of simple perturbation theory, in particular the second-order expression for the interaction of two levels:[20]

$$\Delta E=\frac{|H_{ij}|^2}{E_i^\circ-E_j^\circ}$$

Computational Details

We model the silver metal substrate by a cluster of three layers of atoms. The three layer model has been shown to

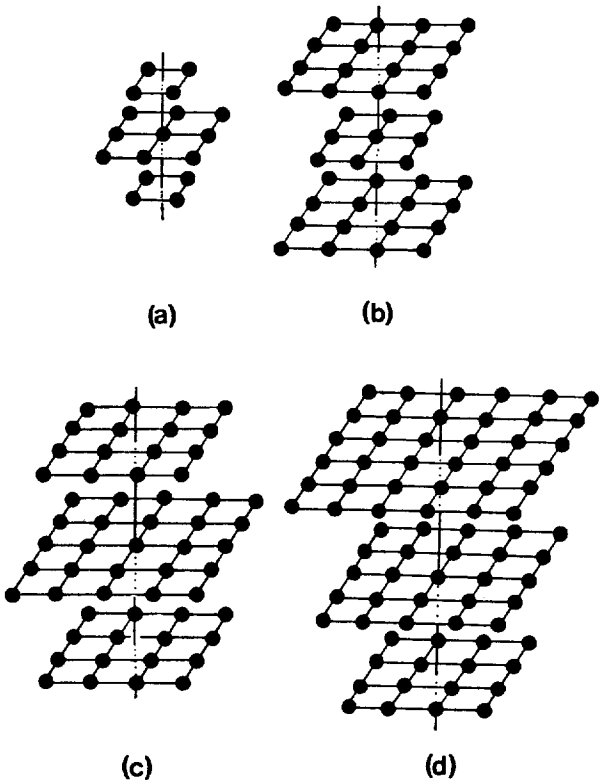

Figure 1. The geometry of silver clusters. (a) Ag_{17}(4, 9, 4) cluster, (b) Ag_{41}(16, 9, 16) cluster, (c) Ag_{57}(16, 25, 16) cluster, and (d) Ag_{77}(36, 25,16) cluster. The 57- and 77-atom clusters are used to show the convergence with size.

Table 1. Extended Hückel Parameters

Orbital	H_{ii}	ζ_1^a	ζ_2^a	c_1^b	c_2^b
Ag 5*s*[c]	−11.10	2.244			
Ag 5*p*[c]	− 5.80	2.202			
Ag 4*d*[c]	−14.50	6.070	2.6630	0.55910	0.60476
H 1*s*	−13.60	1.30			
C 2*s*	−21.40	1.625			
C 2*p*	−11.40	1.625			
S 3*s*	−20.0	1.817			
S 3*p*	−13.3	1.817			
S 3*d*	−8.0	1.500			

[a] exponents in a double-ζ expansion of the metal *d* orbitals. [b] coefficients in a double-ζ expansion of the metal *d* orbitals. [c] Reference 24.

be a reasonable compromise between a convenient size of the calculation and an adequate representation of the surface.[20] We use 17 atom and 41 atom clusters. The geometry is given in Figure 1.

The Ag-Ag distance is taken as 2.89 Å, which is the nearest neighbour distance in bulk silver.[21] Since it is well established that the methanethiol is adsorbed on metal surface dissociatively with S-H bond ruptured, we assume the methanethiolate radical ($CH_3S\cdot$) as adsorbate. But we'll show that the results are not quite different even if we take the methanethiolate anion (CH_3S^-) as the adsorbate. The methanethiolate on silver surface is assumed to have the identical geometry as under the isolated condition. The geometry of the isolated methanethiolate is taken from the *ab-initio* calculation of Magnusson.[22] We take the Ag-S distance to be 2.38 Å, which is found in Ag complex.[23] The EH parameters used in the calculation are collected in Table 1. The parameters for Ag are taken from the calculation of R. Hoffmann on the O_2 chemisorption on a Ag(110) surface.[24]

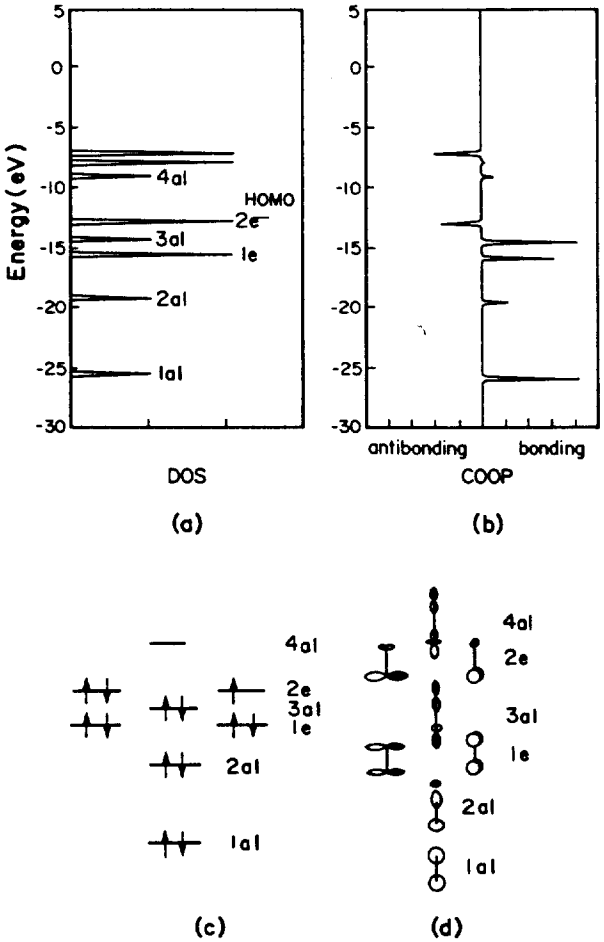

Figure 2. (a) DOS curve of isolated methanethiolate radical. The arrow indicates the HOMO position before adsorption. (b) The C-S COOP curve of isolated methanethiolate radical. The positive regions are bonding, and the negative regions are antibonding. (c) The energy level diagram of methanethiolate radical, the 2e energy level is partially filled. (d) The orbital shape of some MO of methanethiolate radical. For simplicity only the C-S bond is shown.

Results and Discussion

First, we have calculated for the isolated methanethiolate radical. The density of states (DOS) curve and the crystal orbital overlap population (COOP) curve are shown in the Figure 2. The COOP of *A-B* bond is defined as follows:

$$\text{COOP } dE = 2\delta(E-E_a) \sum_{i\in A} \sum_{j\in B} C_{ia} C_{ja} S_{ij} dE \quad (1)$$

$$= \frac{2}{(\pi\sigma^2)^{1/2}} \sum_{i\in A} \sum_{j\in B} C_{ia} C_{ja} S_{ij} \exp[-(E-E_a)^2/(2\sigma^2)] dE \quad (2)$$

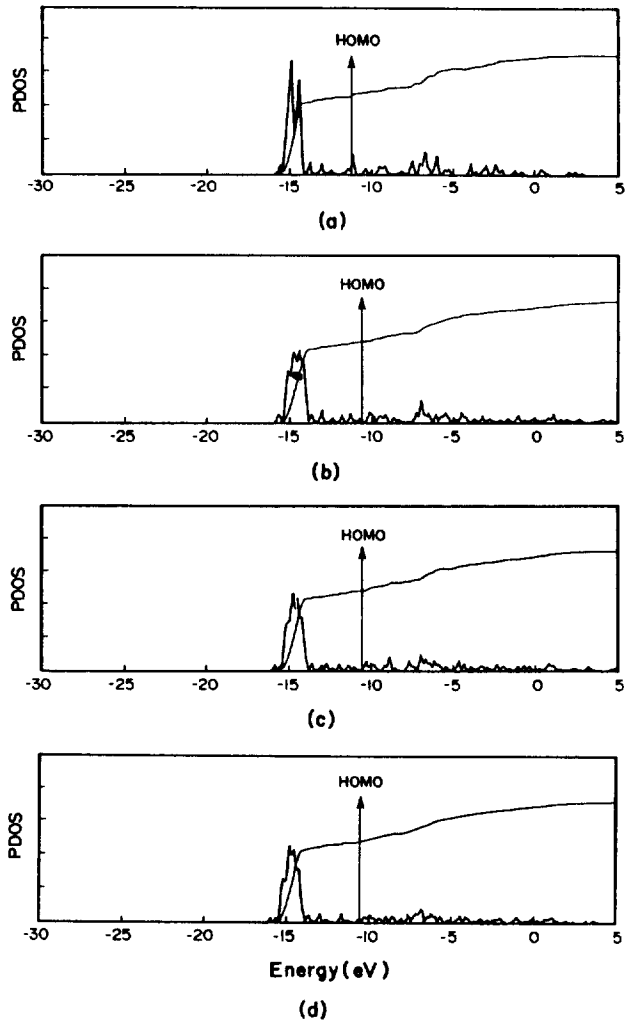

Figure 3. The PDOS curves onto the 4 atoms near the 4-fold adsorption site of (a) Ag_{17} cluster, (b) Ag_{41} cluster, (c) Ag_{57} cluster, and (d) Ag_{77} cluster. The heavy solid line is the PDOS curve, the solid line is the integrated PDOS, and the arrow indicates the HOMO energy level.

where $C_{i\alpha}$ is the ith coefficient of αth MO and S_{ij} is an overlap integral of ith basis and jth basis. A and B could be atoms or fragments. The COOP is an overlap-population-weighted density of states, *i.e.*, the relative number in a given energy interval weighted by the contribution these levels make to the overlap population for a specified bond[25] and shows the contribution of orbitals to the bonding of two specified atoms. The positive regions of the COOP curve signify bonding and negative regions represent antibonding. The amplitude of the curve depends on the number of states in the energy interval, the magnitude of the coupling overlap, and the size of the coefficients in the MO's.[26] In Figure 2, molecular orbital diagram and orbital shapes of isolated $CH_3S\cdot$ are shown together. The $1a_1$ is a bonding orbital between the s orbitals of carbon and sulfur. The $2a_1$ is bonding orbital between the sp_z hybridized orbitals of carbon and sulfur. The $1e$ orbitals are degenerate ones with bonding character which are composed of p_x, p_y orbitals of carbon and sulfur (π type orbital). The $3a_1$ is a bonding orbital which is made of sp_z hybridized orbitals of carbon and sulfur. The $2e$ orbitals are degenerate antibonding orbitals between p_x, p_y of carbon and sulfur of which the major component is from sulfur (almost nonbonding sulfur p_x, p_y orbitals). The $4a_1$ orbital is mainly composed of p_z orbital of carbon and s, p_z, and d_{z^2} of sulfur. It has a bonding character. The 3e orbitals are $d_{x^2-y^2}$ and d_{xy} of sulfur, respectively, and have nonbonding character.

Before proceeding to the composite system of the adsorbate and substrate, it is necessary to check that our 41 atom cluster is large enough to represent the metal surface. For this purpose we have carried out the calculation of the clusters of various size Ag_{17}, Ag_{41}, Ag_{57} and Ag_{77} clusters. The geometry is shown in Figure 1. Since the chemisorption is known to be a local phenomenon and to be modified by the nonlocal properties such as the band structure and the work function, we have paid attention to only the atoms near the adsorpion site to see the convergence. Since we choose the 4-fold hollow site as the adsorption site as will be shown later, we focused on the 4 atoms near the 4-fold hollow site. In Figure 3, the projections (PDOS) onto the 4 atoms of

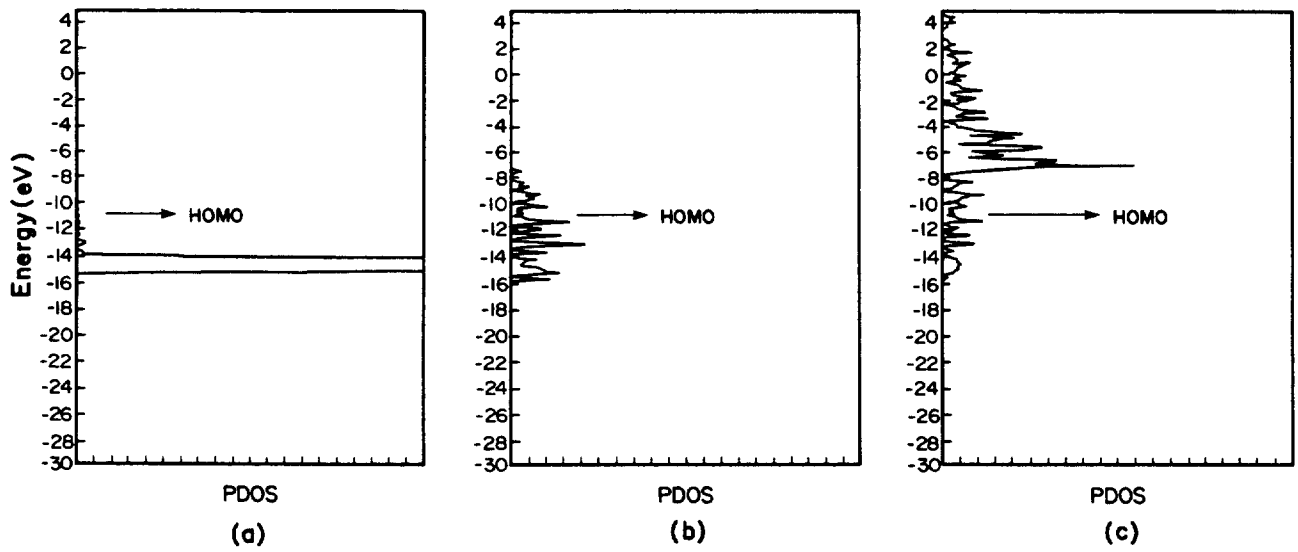

Figure 4. The PDOS of Ag orbitals Ag_{41} cluster. (a) 4*d*, (b) 5*s*, and (c) 5*p*. The arrow indicates the HOMO energy level. Near the HOMO 4d orbitals have little contribution.

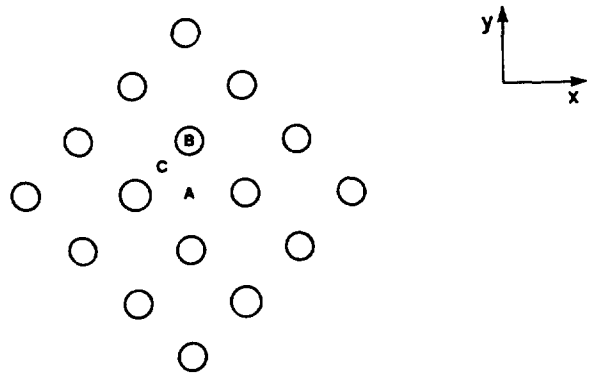

Figure 5. Adsorption sites of Ag(100) plane. A: 4-fold coordinated hollow site, B: 1-fold cooridanted on-top site, and C: 2-fold coordinated bridge site.

Table 2. Calculated Binding Energy (BE) and the Reduced Overlap Populations (ROP) on Various Adsorption Sites
(a) $CH_3S\cdot$ adsorbed on Ag_{41} cluster

Site	BE(eV)[a]	ROP(C-S)[b]	ROP(ads.- sub.)[c]
on-top	3.93	0.819	0.644
bridge	4.98	0.827	1.177
hollow	6.29	0.830	2.071

(b) $CH_3S\cdot$ adsorbed on Ag_{17} cluster

Site	BE(eV)[a]	ROP(C-S)[b]	ROP(ads.- sub.)[c]
on-top	3.84	0.817	0.647
bridge	5.01	0.826	1.195
hollow	5.72	0.838	2.048

[a] BE = binding energy = $E(CH_3S)+E(Ag\ cluster)-E(CH_3S\cdot/Ag\ cluster)$. [b] reduced overlap population of C-S bond of $CH_3S\cdot$, ROP (C-S) = 0.848 for free CH_3SH, 0.861 for free CH_3S. [c] reduced overlap population between adsorbate and substrate(Ag metal).

DOS of each cluster are shown. The PDOS shows the contribution of a certain fragment (orbital or atom) of system to the total DOS. The PDOS for the Ag_{41} cluster is hardly distinguishable from those of Ag_{57} and Ag_{77} clusters. Thus we carry out the calculation with the Ag_{41} cluster.

In Figure 4 we give the projections (PDOS) onto 4*d*, 5*s* and 5*p* components of DOS of Ag_{41} cluster. Near the Fermi level (HOMO) considered to be important in the interaction with adsorbate, most contribution comes from 5*s* orbitals. That is, the silver 5*s* should be mostly responsible for interaction with adsorbate. But the contribution of 4*d* and 5*p* may not be entirely ignored.

The possible adsorption sites of f.c.c. Ag(100) surface are 1-fold coordinated on-top, 2-fold coordinated bridge and 4-fold coodinated hollow sites. These are drawn in Figure 5. We have performed the calculation for the $CH_3S\cdot$ adsorbed on these sites. Table 2 gives some calculation results-binding energy, and reduced overlap populations. The reduced overlap population (ROP) of a bond is defined as follows:

$$\mathrm{ROP}=2\sum_{\alpha}\sum_{i\in A}\sum_{i\in B} n_\alpha C_{i\alpha} C_{j\alpha} S_{ij} \qquad (3)$$

Table 3. Calculated Binding Energy and Reduced Overlap Population at Various Tilt Angle
(a) $CH_3S\cdot$ adsorbed on Ag_{41} cluster

Tilt angle	BE(eV)	ROP(C-S)[a]
0°	6.71	0.848
15°	6.62	0.843
30°	6.30	0.830
45°	5.72	0.813

(b) $CH_3S\cdot$ adsorbed on Ag_{17} cluster

Tilt angle	BE(eV)	ROP(C-S)[a]
0°	5.89	0.838
15°	5.87	0.838
30°	5.73	0.838
45°	5.40	0.840

[a] ROP(C-S) = 0.848 for free CH_3SH, 0.861 for free CH_3S.

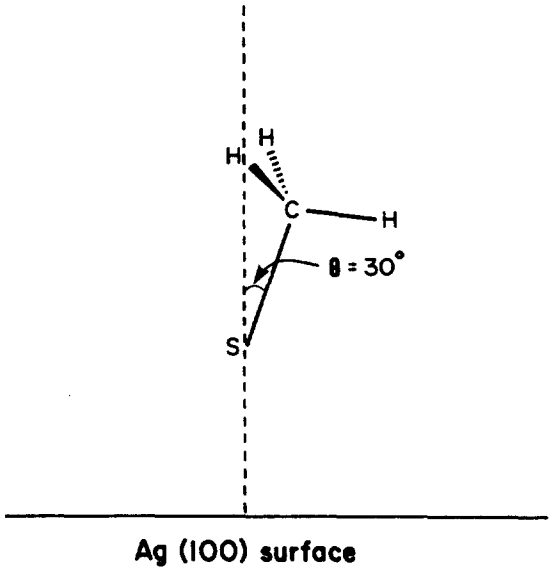

Figure 6. Geometry of $CH_3S\cdot$ adsorbed on Ag surface. The C-S bond is tilted by 30° from the surface normal($\theta = 30°$).

where n_α is the occupation of the αth MO. It has been used successfully as an indication of the strength of a given bond and has been correlated with such properties as force constants, vibration frequencies, and dissociation energies.[27] The result shows that the adsorbate is most stable on the 4-fold hollow site. It can be rationalized by the fact that the character of HOMO of methanethiolate is of *e*-symmetry. These orbitals can be stabilized by the interaction with the silver MO of the same symmetry, *i.e.*, *e*-symmetry. These are located broadly near the Fermi level. Thus there are the interactions between unoccupied MO and occupied MO, which play a central role in bonding. But on the on-top site, from symmetry, the $2e$ (HOMO) do not interact with metal, but MO's with a_1-symmetry are responsible for the interaction between adsorbate and substrate. However the $2a_1$ and the $3a_1$, considerably below the HOMO level, lead only to the occu-

Table 4. The Binding Energy and Reduced Overlap Population for the Different Directions to which the C-S Bond of $CH_3S\cdot$ is Tilted

(a) on Ag_{41} cluster

Direction	BE(eV)	ROP(C-S)[a]
[100]	6.30	0.830
[110]	6.36	0.834

(b) on Ag_{17} cluster

Direction	BE(eV)	ROP(C-S)[a]
[100]	5.73	0.838
[110]	5.75	0.839

[a] ROP(C-S)=0.848 for free CH_3SH, 0.861 for free $CH_3S\cdot$

pied MO-occupied MO interactions with metal and therefore these contributions to the bonding are small. The $4a_1$, which is in much higher energy region than the HOMO level, leads only to unoccupied MO-unoccupied MO interaction with metal and contributes little to the bonding to the metal. Thus the methanethiolate is not stabilized much at the on-top site. There is no experimental data about the preferred adsorption site of CH_3S/Ag system. However for the CH_3O/Cu, which is considered to have similar chemical property, the adsorbate is found to be adsorbed on the hollow site or bridge site.[28] Thus we consider only the 4-fold hollow site.

Form experiments, the methanethiolate has been known to be adsorbed on Cu and Pt with the tilted C-S bond from the surface normal.[10,12] The calculation is carried out for the different polar angles θ of C-S bond from the surface normal. It appears from Table 3 that there's no preference in the polar angle within our calculational accuracy because the energy difference is too small. Thus we assume that the adsorbate C-S bond is tilted by 30° from the surface normal from the result observed on copper surface.

The azimuthal angle dependence is also considered, *i.e.*,

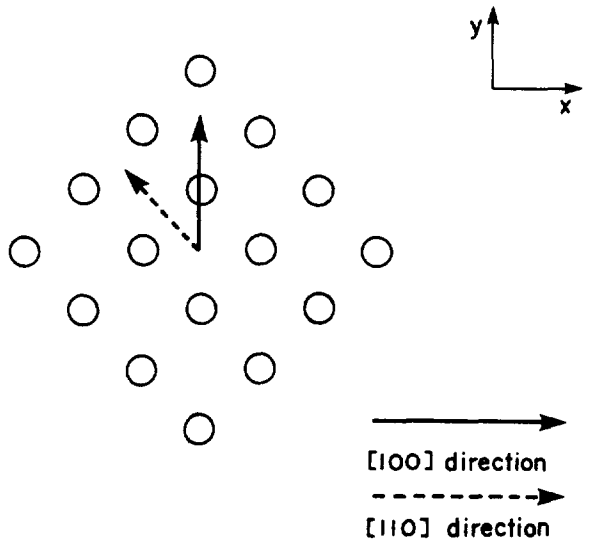

Figure 7. The direction in which the C-S bond of $CH_3S\cdot$ is tilted.

in which direction the C-S bond is tilted- [100] or [110] direction? The result is given in Table 4. One finds that the repulsion between Ag and C leads to the conformation that the two atoms are far apart. However, the energy difference is so small that no specific conformation exists. In Figure 8, the projected density of state (PDOS) of the $CH_3S\cdot$ MO is drawn for the [100] and [110] directions. The PDOS pattern is useful in tracing the change of a certain fragment occurred during the chemical events. It appears from Figure 8 that the chemisorption nature in each direction is almost identical. Thus we consider only the [100] direction from now on.

In Figure 8, the PDOS curves for the Ag_{17} and Ag_{41} clusters are given together for comparison. The peak patterns for the two cases are hardly distinguishable. And as shown in Table 3 and 4, the qualitative nature of the adsorption for the two cases is not quite different. Thus we carry out

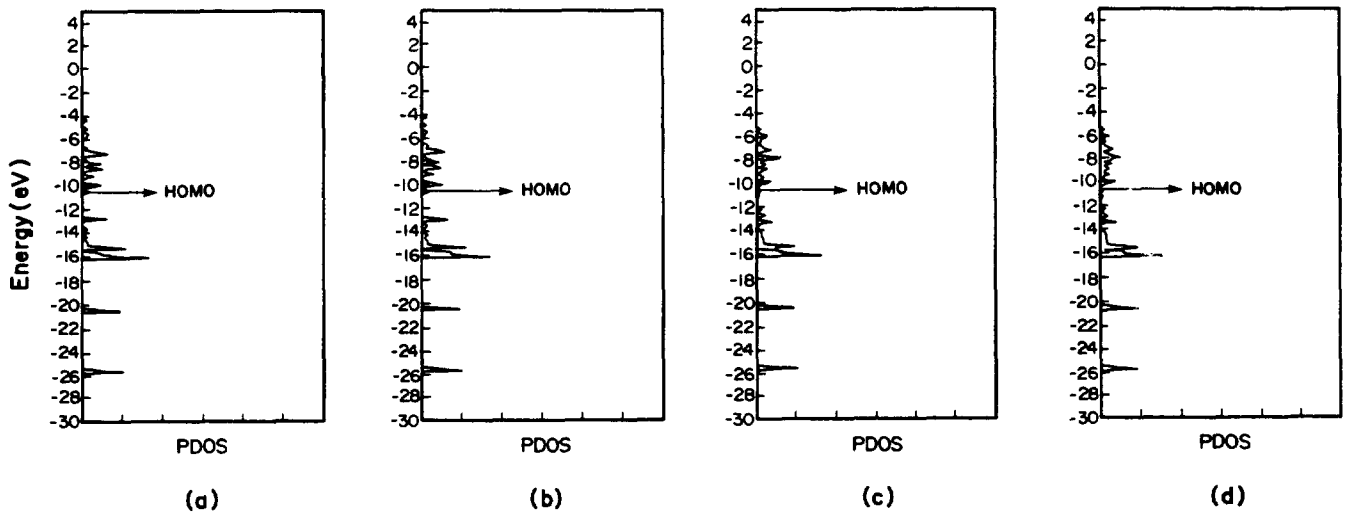

Figure 8. The projected density of states (PDOS) onto all the adsorbate states (a) of $CH_3S\cdot/Ag_{17}$ with C-S bond tilted in the [100] direction, (b) of $CH_3S\cdot/Ag_{17}$ with C-S in the [110], (c) of $CH_3S\cdot/Ag_{41}$ with C-S in the [100], and (d) of $CH_3S\cdot Ag_{41}$ with C-S in [110].

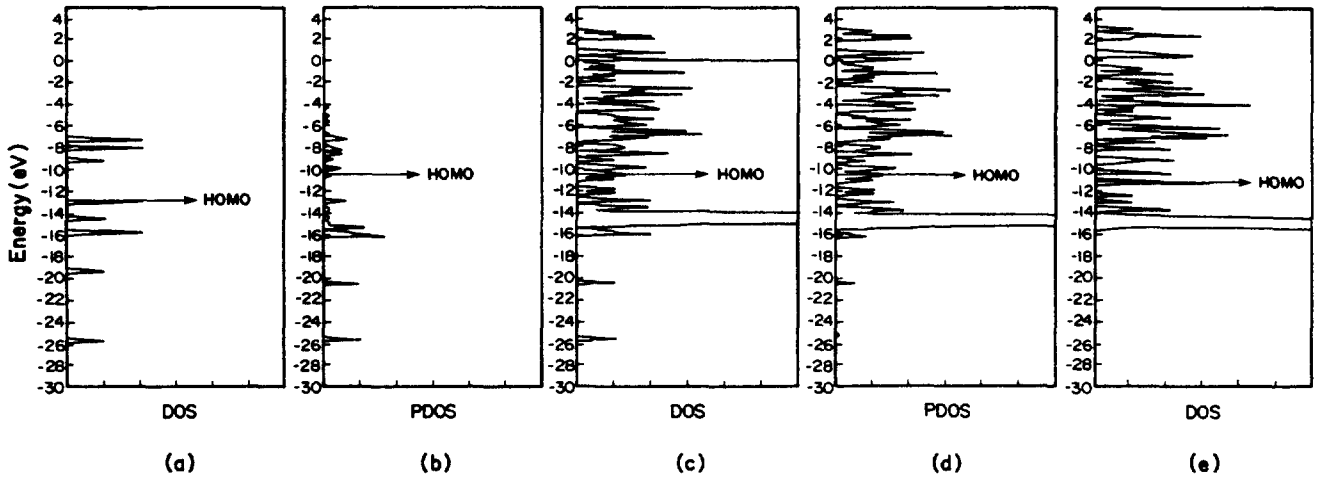

Figure 9. (a) The total DOS of $CH_3S\cdot$ before adsorption. (b) The projected DOS onto $CH_3S\cdot$ after adsorption on Ag_{17} cluster. (c) The total DOS of $CH_3S\cdot/Ag_{17}$ cluster after adsorption. (d) The projected DOS onto Ag_{17} cluster after adsorption. (e) The total DOS of Ag_{17} cluster before adsorption. The arrow indicates the HOMO energy level.

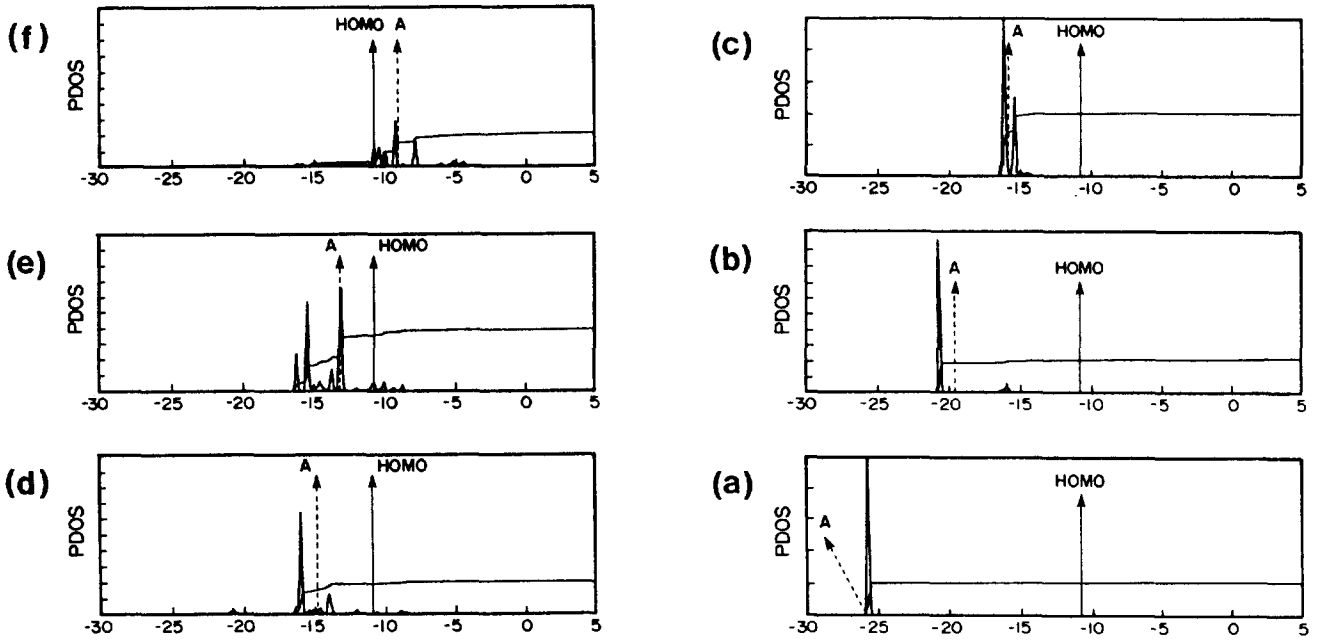

Figure 10. The projection onto each state of $CH_3S\cdot$ of DOS of $CH_3S\cdot/Ag_{17}$ cluster (4-fold hollow site). The integration is shown together. The integrated value up to the HOMO is proportional to the population of the state. The solid arrow indicates the HOMO energy level. The dashed arrow indicates the original position of the state before adsorption. (a) $1a_1$, (b) $2a_1$, (c) $1e$, (d) $3a_1$, (e) $2e$, and (f) $4a_1$ level.

more detailed analysis for the adsorption on the 17-atom cluster.

We show in center of Figure 9 (Figure 9(c)) the total DOS of $CH_3S\cdot/Ag$, in Figure 9(b) the projection (PDOS) of all the adsorbate states and in Figure 9(d) the projection (PDOS) of all the substrate states. The DOS's of an isolated adsorbate and of an isolated substrate are depicted in Figure 9(a) and 9(e), respectively, for comparison. One can see more easily the changes in the adsorbate states than in the substrate states. Comparing (a) with (b), the peaks below -15 eV seem to be unchanged during the adsorption. However, comparing Figure (d) with (e), one sees two clear new peak (*ca.* -20 eV and -16 eV) in PDOS of the substrate states after the adsorption. The equal position of these peaks in (b) and (d) indicates that these come from the interaction of the methanethiolate with metal. Comparing (a) with (b), one finds that some peaks of the adsorbate, especially above -15 eV, spread out broadly. It comes from the interaction with the metal band.

To understand which orbitals are involved in the bonding we must consider the projections of each of them. Figure 10 shows the projections (PDOS) of each MO of $CH_3S\cdot$ in DOS of $CH_3S\cdot/Ag_{17}$ cluster. Comparing the peaks with the original one of the isolated adsorbate, the changes due

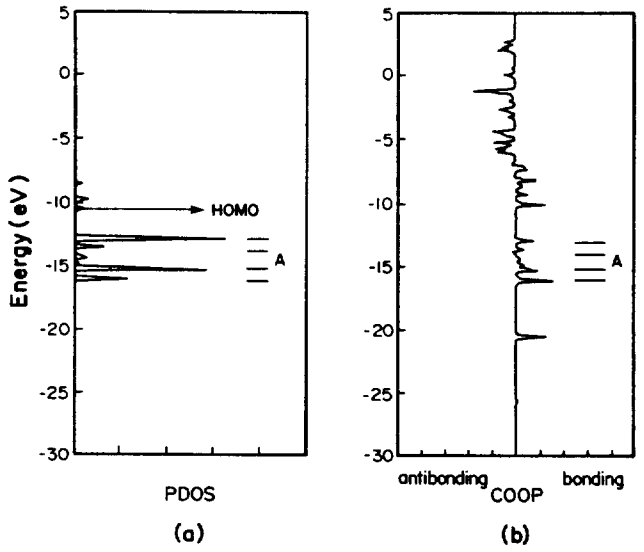

Figure 11. (a) The PDOS curve of $2e$ of $CH_3S\cdot$. (b) The COOP curve of S-Ag bond for the $CH_3S\cdot/Ag_{17}$ cluster. The arrow indicates the HOMO level and the solid lines (A) are marked to show the coincident peak positions of the two curves. It shows that the $2e$ contributes mainly to the adsorbate-substrate bonding.

to the adsoption are easily grasped. The $1a_1$ MO is almost at the original position and not perturbed because there is a large energy gap with metal band (See Figure 9(a) and (e)). When the methanethiolate is adsorbed on the Ag cluster with the C-S bond tilted by 30° in the y-direction ([100] direction), the C_{3v} symmetry of isolated methanethiolate is reduced to C_s symmetry ($a_1\rightarrow a'$, $e\rightarrow a'+a''$). The $1e$ are splitted to a' and a'', and the MO of p_y character (a') of e orbitals is rehybridized with the p_z orbital (a'). However, it is known that, with C-S bond tilted by 30°, the degeneracy is hardly removed and the extent to this rehybridization is small.[12] Because of its large energy difference from e orbitals of metal, the $1e$ is little perturbed except for this splitting that comes from the reduction of its symmetry due to the adsorption. For the $2a_1$ and for the $3a_1$, the main peaks shift to the lower energy from the interaction with the silver. Since the a_1-symmetric metal MO lies near the bottom of band (*ca.* -15 eV), the interaction of $2a_1$ and of $3a_1$ with these metal orbitals is between the occupied MO's and contributes little to the bonding. Although there are some a_1-symmetric components in the energy region higher than HOMO level, the interaction of $2a_1$ and $3a_1$ with these is small because of the large energy gap. The $2e$ (HOMO) interacts with the metal e orbitals, which are located widely near the Fermi level. Since the $2e$ is also located near the Fermi level of metal (See Figure 9(a) and (e)), this interaction is large and the $2e$ is dispersed broadly after adsorption as show in Figure 10(e). The interaction of $2e$ with the occupied level of the metal lead to the metal-to-adsorbate charge-transfer since the $2e$ level of the adsorbate is partially occupied (See the integration curve of Figure 10(e)). This interaction is the major factor for the $CH_3S\cdot$-Ag bonding. This is confirmed with the fact that the peak of Ag-S COOP coincide with the peak of the PDOS of the $2e$ MO (See Figure 11). The $4a_1$ MO has the a'-symmetry and interact with the metal

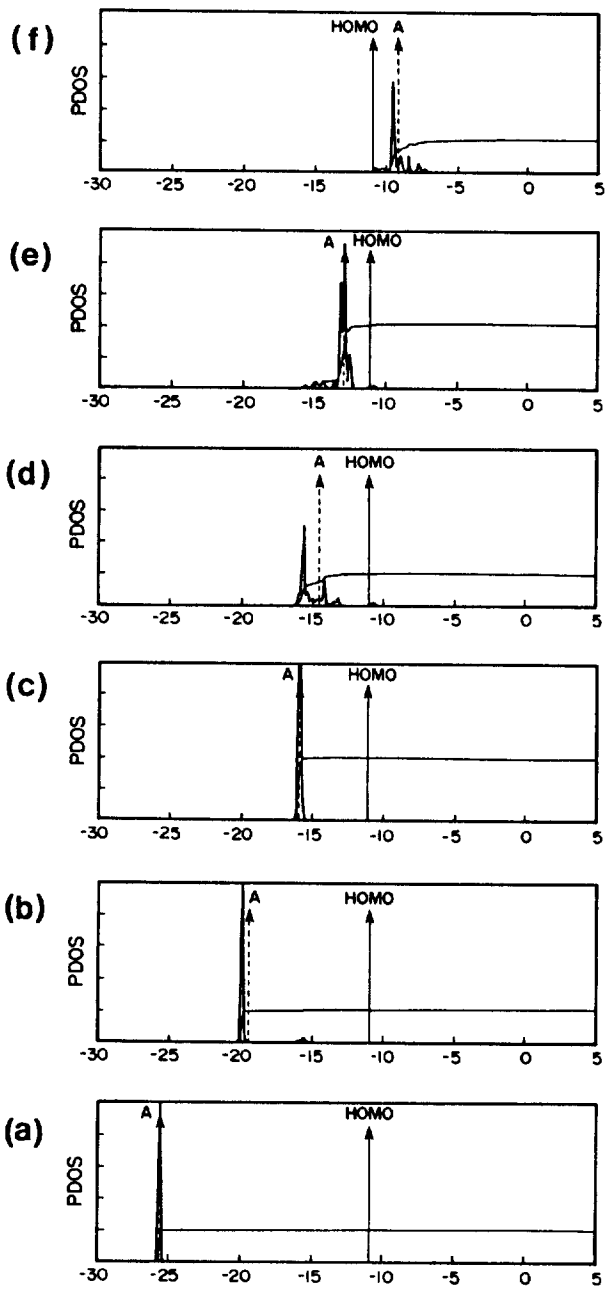

Figure 12. The projection onto each state of $CH_3S\cdot$ of DOS of $CH_3S\cdot/Ag_{17}$ cluster (on-top site). The integration is shown together. The solid arrow indicates the HOMO energy level. The dashed arrow indicates the original position of the state before adsorption. (a) $1a_1$, (b) $2a_1$, (c) $1e$, (d) $3a_1$, (e) $2e$, and (f) $4a_1$ level.

MO of the same symmetry. Some metal MO's with a' symetry are located near the Fermi level and the interaction of the unoccupied $4a_1$ MO with these metal MO contributes to the back donation from the metal to adsorbate and the occupation of $4a_1$ increases slightly.

The PDOS of each MO of methanethiolate on the on-top site of Ag cluster is given in Figure 12 for the comparison with the above result on the hollow site. The $2e$, which was the major factor of bonding on the hollow site, is little

Table 5. The Change of Reduced Overlap Population of C-S bond of Methanethiol Due to Adsorption
(a) along the radical pathway

States	ROP(C-S)
CH_3SH	0.848
$CH_3S\cdot$	0.861
$CH_3S\cdot$ /Ag	0.830

(b) along the anionic pathway

States	ROP(C-S)
CH_3SH	0.848
CH_3S^-	0.825
CH_3S^-/Ag	0.830

perturbed on the on-top site. The $3a_1$ and the $4a_1$ spread out broadly and seem to play a central role in the interaction with metal. However, the interactions are between occupied levels or between unoccupied levels. Thus these contribution to the bonding is small. This explains the result that the methanethiolate is favoured on the hollow site over the on-top site.

As seen in the C-S COOP curve of the Figure 2, the $3a_1$ MO has a large bonding character between carbon and sulfur. Thus the slight depopulation of electrons from this MO may lead to the considerable weakening of the C-S bond. The $4a_1$ MO has very weak C-S bonding character and the extent to the bond-strengthening by the population of the level is very small. But the change of the population of $3a_1$ and $4a_1$ is very small and their contribution to the bond order change of the C-S bond is relatively small compared with that of $2e$. The $2e$ MO's have antibonding character. The charge-transfer to these energy states, which comes from the interaction between adsorbate and substrate, results in the weakening of the C-S bond. So we are convinced that the interactions with the metal lead to the weakening of the C-S bond. This is reflected in the change of reduced overlap population (ROP). During the adsorption, the ROP of the C-S bond decreases compared with that of the isolated methanethiolate radical C-S bond and that of the isolated methanethiol C-S bond (See Table 5). This result is consistent with the SERS experimental result of red shift in the C-S stretching frequency.

So far, the adsorbate has been assumed to be present in the form of radical on metal surface. The adsorbed species may be an anion by the action of oxidizing reagent in some experimental condition. We also calculated on this case. Table 5 shows the ressult for this case. As shown schematically in Figure 13, we simply consider that the adsorption of methanethiol on metal surface proceeds in two steps- S-H bond rupture as the first step and adsorption as the seconds step. Depending upon the species produced by the S-H bond rupture, radical or anion, we call it the anionic pathway or the radical one. In Figure 13, the ROP at each stage is give together to show the change of bond order during the adsorption process. In the anionic pathway (a), the stage of formation of anion is the major cause to the bond weakening from the transfer of an electron to the C-S antibonding orbi-

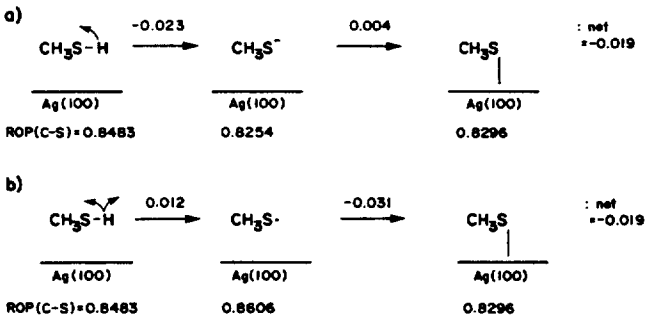

Figure 13. A schematic diagram for the adsorption process of methanethiol on Ag surface, which is simply assumed to proceed in two steps: S-H rupture and adsorption. The two different adsorption pathways are considered. (a) The anionic pathway. The adsorbate is adsorbed on the Ag surface in the form of anion. (b) The radical pathway. The adsorbate adsorbed on the Ag surface on the form of radical. The ROP of C-S bond of each stage is shown together.

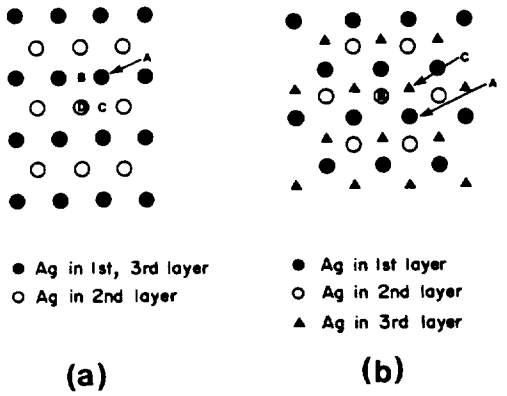

Figure 14. The geometry of the clusters used to represent Ag (110) and Ag(111) surfaces. The three layer clusters are used. The adsorption sites of each plane are shown together. (a) Ag_{41} (16, 9, 16) for the (110) surface(A: on-top, B: short-bridge, C: long-bridge, D: hollow site) (b) Ag_{35}(14, 7, 14) for the (111) surface (A: on-top, B: hollow, C: hollow site)

Table 6. The Binding Energy and Overlap Population for the CH_3S on Ag(111) and Ag(110) Surface
(a) on Ag(111) surface

Site	BE(eV)	ROP(C-S)[b]	ROP(ads.- sub.)
on-top(A)[a]	3.40	0.818	0.641
hollow(B)	5.38	0.821	1.611
hollow(C)	5.37	0.829	1.623

(b) on Ag(110) surface

Site	BE(eV)	ROP(C-S)[b]	ROP(ads.- sub.)
on-top(A)[a]	3.54	0.818	0.636
Shor bridge(B)	4.86	0.834	1.200
Long bridge(C)	4.42	0.810	1.349
Hollow(D)	3.21	0.837	1.300

[a] See Figure 14. [b] ROP(C-S)=0.848 for free CH_3SH, 0.861 for free $CH_3S\cdot$

Table 7. MNDO- and EH-Calculated HOMO Energies (eV) and Nature

	MNDO	EHT	HOMO nature
CH_3SH	−10.290	−12.833	
CH_3CH_2SH	−10.241	−12.423	C-S antibonding
$(CH_3)_2SH$	−10.234	−12.563	(almost p_x and p_y of slufur)
$CH_3(CH_2)_2SH$	−10.267	−12.832	
$CH_3(CH_2)_3SH$	−10.260	−12.780	
CH_3SCH_3	−10.026	−12.562	C-S antibonding
$CH_3CH_2SCH_2CH_3$	−10.006	−12.424	(almost p_x and p_y of slufur)

tal $2e$. In the radical pathway (b), the stage of adsorption plays the central role in the C-S bond weakening as shown so far. Thus in both cases the methanethiol C-S bond is weakened when it is adsorbed on the Ag cluster and this is consistent with the experimental result, *i.e.*, the red shift of the C-S stretching frequency.

We also have carried out the calculations for the Ag(110) and Ag(111) planes. The geometries of the clusters used in the calculation are shown in Figure 14. The results are given in Table 6. The bridge or hollow sites are preferred over the on-top site and the C-S bond in methanethiolate is weakened as the above results on the Ag(100) cluster. Thus the methanethiolate shows almost the identical behaviour on the three different planes.

Since it is well established that the S-S bond of dislufide is cleavaged on the silver,[29-31] our calculation results may also be applicable to the explanation of the adsorption of disulfide.

Conclusion

An EH calculation is carried out for the methanethiolate on silver clusters. We have shown that the methanethiolate radical interacts with the silver cluster mainly through HOMO, *i.e.*, $2e$ orbital. The methanethiolate radical preferred the highly coordinated site to the on-top site. The C-S bond is weakened by the increase in the population of the $2e$ level. This bond weakening is consistent with the experimental result of red shift of the C-S stretching frequency.

Acknowledgement. The work was supported by the Ministry of Educations, Republic of Korea.

Appendix

Some aliphatic sulfur-containing molecules have similar HOMO energy and nature. Some MNDO and EH calculation results are collected in Table 7.

Reference

1. T. H. Joo, K. Kim, and M. S. Kim, *J. Mol. Struct.*, **162**, 191 (1987).
2. C. K. Kwon *et al.*, *Bull. Korean Chem. Soc.*, **10**, 254 (1989).
3. C. K. Kwon, M. S. Kim, and K. Kim, *J. Raman Spec.*, **20**, 575 (1989).
4. T. H. Joo, M. S. Kim, and K. Kim, *J. Mol. Struct.*, **160**, 81 (1987).
5. C. K. Kwon, M. S. Kim, and K. Kim, *J. Mol. Struct.*, **162**, 201 (1987).
6. T. H. Joo, K. Kim, and M. S. Kim, *J. Mol. Struct.*, **158**, 265 (1987).
7. T. H. Joo, K. Kim, and M. S. Kim, *J. Phys. Chem.*, **90**, 5816 (1986).
8. T. H. Joo *et al.*, *J. Phys. Chem.*, **93**, 1422 (1989).
9. R. J. Koestner *et al.*, *Chem. Phys. Lett.*, **120**, 285 (1985).
10. B. A. Sexton and G. L. Nyberg, *Surface Sci.*, **165**, 251 (1986).
11. D. L. Seymours *et al.*, *Surface Sci.*, **189/190**, 529 (1987).
12. J. T. Roberts and C. M. Friend, *J. Am. Chem. Soc.*, **108**, 7204 (1986).
13. J. T. Roberts and C. M. Friend, *J. Chem. Phys.*, **88**, 7172 (1988).
14. J. T. Roberts and C. M. Friend, *J. Phys. Chem.*, **92**, 5205 (1988).
15. C. P. DeMelo *et al.*, *Phys. Rev. B.*, **35**, 7847 (1987).
16. K. Hermann, P. S. Bagus, and C. J. Nelin, *Phys. Rev. B.*, **35**, 9467 (1987).
17. P. N. Sanda *et al.*, *Phys. Rev. lett.*, **45**, 1519 (1980).
18. S. L. McCall and P. M. Platzman, *Phys. Rev. B.*, **22**, 1660 (1980).
19. M. Moskovits, *J. Chem. Phys.*, **69**, 4159 (1978).
20. (a) J. Y. Saillard and R. Hoffmann, *J. Am. Chem. Soc.*, **106**, 2006 (1986); (b) M. C. Zonnevylle *et al.*, *Surface Sci.*, **223**, 233 (1989).
21. V. I. Moruzzi, J. F. Janak, and A. R. Williams, "Calculated electronic properties of metals", p. 148, Pergamon Press Co., New York, U.S.A., 1978.
22. E. Magnusson, *J. Am. Chem. Soc.*, **108**, 11 (1986).
23. I. G. Dance *et al.*, *Inorg. Chem.*, **22**, 3785 (1983).
24. K. A. Jørgensen and R. Hoffmann, *J. Phys. Chem.*, **94**, 3046 (1990).
25. (a) T. Hughbanks and R. Hoffmann, *J. Am. Chem. Soc.*, **105**, 3528 (1983); (b) M. Kertesz and R. Hoffmann, *J. Am. Chem. Soc.*, **106**, 3453 (1984).
26. R. Hoffmann, *Rev. Mod. Phys.*, **60**, 601 (1988).
27. (a) P. Politzer and S. D. Kasten, *J. Phys. Chem.*, **80**, 385 (1976); (b) T. S. Kusuma and A. L. Companion, *Surface Sci.*, **195**, 59 (1988).
28. T. Linder *et al.*, *Surface Sci.*, **203**, 333 (1988).
29. C. J. Sandroff and D. R. Herschbach, *J. Phys. Chem.*, **86**, 3277 (1982).
30. M. Takahashi, M. Fujita, and M. Ito, *Surface Sci.*, **158**, 307 (1985).
31. T. Watanabe and H. Maeda, *J. Phys. Chem.*, **93**, 3258 (1989).